Scanning Microscopy

Volume 10 | Number 4 Article 5

10-10-1996

Imaging the Electrocyte of Torpedo Marmorata by Scanning Force Microscopy

L. I. Pietrasanta
Max Planck Institute for Biophysical Chemistry

A. Schaper
Max Planck Institute for Biophysical Chemistry

G. Q. Fox
Max Planck Institute for Biophysical Chemistry

F. J. Barrantes
Instituto de Investigaciones Bioquimicas

T. M. Jovin
Max Planck Institute for Biophysical Chemistry, tjovin@mpc186.mpibpc.gwdg.de

Scanning Microscopy Vol. 10, No. 4, 1996 (Pages 963-974) 0891-7035/96$5.00+.25
Scanning Microscopy International, Chicago (AMF O'Hare), IL 60666 USA

IMAGING THE ELECTROCYTE OF *TORPEDO MARMORATA* BY SCANNING FORCE MICROSCOPY

L.I. Pietrasanta[1,3], A. Schaper[1], G.Q. Fox[2], F.J. Barrantes[3], and T.M. Jovin[1,*]

[1]Department of Molecular Biology, and [2]Electron Microscopy Group, Max Planck Institute for Biophysical Chemistry, Göttingen, Germany, [3]Instituto de Investigaciones Bioquimícas (INIBIBB), Bahía Blanca, Argentina

(received for publication July 1, 1996 and in revised form October 10, 1996)

Abstract

Scanning force microscopy (SFM) and scanning electron microscopy (SEM) were used to examine the tissue structure of the electric organ of *Torpedo marmorata* in air and in liquid after applying fracturing and cryosectioning techniques and chemical fixation. The electric organ is organized in columns of stacked electrocytes, arranged in a honeycomb pattern. The columns were cut along a plane normal to the cell stack and thin sections were transferred to polylysine coated glass coverslips. The polarity of the electrocytes was made apparent by immunofluorescence microscopy directed to different domains of the acetylcholine receptor (AChR), thus revealing the innervated face of the cell. SFM and SEM both showed cell surfaces to be overlaid by a network of collagen fibers by their characteristic banding pattern with about 64 nm periodicity and about 2.5 nm corrugation amplitude. In liquid, significantly lower structural resolution was achieved by SFM, probably due to sample elasticity.

Key Words: Atomic force microscopy, scanning electron microscopy, tissue structure, collagen.

*Address for correspondence:
T.M. Jovin
Department of Molecular Biology,
Max Planck Institute for Biophysical Chemistry,
Am Fassberg 11,
D-37077 Göttingen, Germany
Telephone number: +49-551-201-1381
FAX number: +49-551-201-1467
E-mail: tjovin@mpc186.mpibpc.gwdg.de

Introduction

The electric organ from *Torpedo marmorata* has been regarded as a model system for the study of cholinergic development, innervation and the chemistry of neurotransmitter release (for a detailed introduction see Whittaker, 1992). The subcellular organization of electrocytes from Torpedinidae and Narcinoidae has been investigated by anatomical, physiological, cytochemical and microscope techniques (Cartaud *et al.*, 1995; Kordelli *et al.*, 1986, 1987, 1989; LaRochelle *et al.*, 1990; Luft, 1958; Richardson *et al.*, 1987; Rosenbludt, 1975; Schoffeniels, 1959; Sealock and Kavookijan, 1980; Walker *et al.*, 1985). The adult electric organ extends from the dorsal to the ventral side of the animal. Electric organs are rather gelatinous, and a large fraction of their volume consists of extracellular space, containing a considerable amount of connective and other accessory tissues as well as blood vessels and motor nerves (Bennett, 1971). Removal of the skin reveals individual columns in a honeycomb arrangement. Each column is composed of a stack of thin horizontally flattened, disc-shaped multinuclear cells, the electrocytes, which exhibit a striking functional and structural polarity. The electrocytes possess a dorsal, non-innervated and a ventral richly-innervated cell membrane (Bennett, 1971; Whittaker, 1992). The former is rich in the Na^+, K^+ ATPase and chloride channels and the latter in the acetylcholine receptor (AChR) (Baumann *et al.*, 1970; Miller, 1983; White and Miller, 1979). Both the dorsal and ventral membranes are highly invaginated and the whole cell is invested with a prominent basal membrane that fills the synaptic cleft and continues around the dorsal face, penetrating into the deepest invaginations and lining their walls (Whittaker, 1992). A layer of collagen covers the outer dorsal and ventral surface of the electrocyte and is colocalized with small nerve fibers and with blood vessels (Sheridan, 1966; Whittaker, 1992).

Since its inception in 1986, scanning force microscopy (SFM) has become a powerful tool for the investigation of cell morphology and subcellular structures (Hansma and Hoh, 1994; Lal and John, 1994). The

SFM offers the potential for atomic/molecular resolution of cellular and molecular structures in air and in liquid (Henderson, 1994; Hoh and Hansma, 1992; Shao *et al.*, 1996), even with living cells under physiological conditions (Barbee *et al.*, 1994; Lal *et al.*, 1995; Shroff *et al.*, 1995). SFM has been applied to studies of the cell membrane, cell organelles, and the cytoskeleton of fixed and living cells (Chang *et al.*, 1993; Hörber *et al.*, 1992; Kasas *et al.*, 1993; Parpura *et al.*, 1993a,b; Pietrasanta *et al.*, 1994; Putman *et al.*, 1993a,b; Radmacher *et al.*, 1992; Vater *et al.*, 1995).

In this study, we investigated structural features of thin sections of the electric organ from *Torpedo marmorata* with a combination of various techniques: scanning force microscopy (SFM), scanning electron microscopy (SEM), and immunofluorescence microscopy (IFM).

Materials and Methods

Biological material

Adult *Torpedo marmorata* were obtained from the Institut de Biologie Marine at Arcachon, France, and kept alive in Göttingen in an artificial sea water aquarium maintained at 18°C. All animals were anesthetized with ethyl-*m*-aminobenzoate (0.5 mg/ml in sea water, Sigma, Deisenhofen, FRG) and killed by spinal section. The electric organ was crudely dissected into small pieces of about 1 cm^3.

Sample preparation from electric organ

Dissected pieces from the electric organ were sliced transversally and longitudinally with respect to the stack of electrocytes.

Transversal cross-sectioning and cryoslicing. Electric organ samples were fixed in 5% glutaraldehyde buffered at pH 7.4 with 0.4 M sodium cacodylate for 2 hours at room temperature. The fixed sample was washed in buffer for 1 hour and postfixed with 1% osmium tetroxide in cacodylate buffer. The sample was dehydrated in increasing concentrations of ethanol (50-100%) and critical point dried (Critical Point Dryer, Balzers, Liechtenstein) in either ethanol or acetone using CO_2 as the transition fluid. Transversal cross-sectioning was performed with a razor blade after critical point drying of the sample.

For cryoslicing, samples of electric organ were fixed with 4% paraformaldehyde, buffered to pH 7.4 by phosphate-buffered saline (PBS), for 2 hours at 4°C. The tissue was impregnated with increasing concentrations of sucrose (5%, 10%, 20% wt/vol in PBS), and then rapidly frozen according to the procedure of Kordelli *et al.* (1986). Transverse frozen sections (5-10 μm thick) were cut with a freezing microtome (Cryostat Frigocut Model 2700, Reichert-Jung, Cambridge Instruments, Cambridge, U.K.) at -20°C. Individual sections were mounted onto glass slides coated with either Vectabond (Vector Laboratories, Burlingame, CA) or polylysine. SFM imaging was conducted directly on sections immersed in liquid or on air dried sections.

Longitudinal mechanical fracturing for SEM and SFM. For SEM the critical point dried dissected piece of electric organ (see above) was mechanically fractured longitudinally with tweezers and attached to a specimen stub with double sided sticky tape. For SFM, dissected columns of prefixed and frozen tissue were cut transversally with a razor blade in slices of about 4-5 mm thickness. The slices were mounted between polylysine-coated coverslips and transferred to a metallic basket used for critical point-drying. After fixation in the vapor phase of 25% glutaraldehyde at 4°C for 2 days, the slices were dehydrated in increasing concentrations of ethanol prior to critical point drying (see above). The coverslips were carefully separated such that part of the tissue remained attached to the glass. The surface was contacted with sticky tape to produce a freshly cleaved surface suitable for SFM (Pietrasanta *et al.*, 1994).

Scanning Electron Microscopy (SEM) and Scanning Force Microscopy (SFM)

For SEM (Stereoscan 150, Cambridge Instruments, U.K.) samples were sputter coated with gold (Union Sputtering Device, Balzers) in a 0.1 mbar argon atmosphere at 30 mA for 2 minutes, with a specimen distance of 5 cm. SFM measurements were performed with NanoScope II and III-multimode SPMs {Digital Instruments (DI), Santa Barbara, CA}. Scanning was with a G-scanner with a 85 μm × 85 μm (x,y) × 4 μm (z) scan range or with a J-scanner (135 μm × 135 μm × 5 μm). The SFM was operated under ambient conditions (18-27°C, relative humidity 15-40%) in the permanent contact mode (with and without feedback electronics, i.e., in the isoforce mode for measurements of the topography or in the error mode (Fritz *et al.*, 1994; Putman *et al.*, 1992), and in the tapping mode. The error mode provides higher contrast images of the surface relief. We used microfabricated pyramidal shaped Si_3N_4-tips (DI) and conical shaped Si-tips (Ultralever, Park Scientific Instruments, Sunnyvale, CA) integrated into a triangular cantilever with a spring constant of about 0.1 N/m. For tapping, the resonance frequency of the Ultralever was about 160 kHz. The loading force of the tip was always minimized by adjusting the damping amplitude to a minimum value (tapping mode) or by adjusting the setpoint of the optical readout signal to a minimum value (permanent contact mode). The latter typically corresponds to a cantilever bending force as low as 1 nN. The total load of the tip is estimated to be typically 1-2 orders of magnitude higher in air, and is

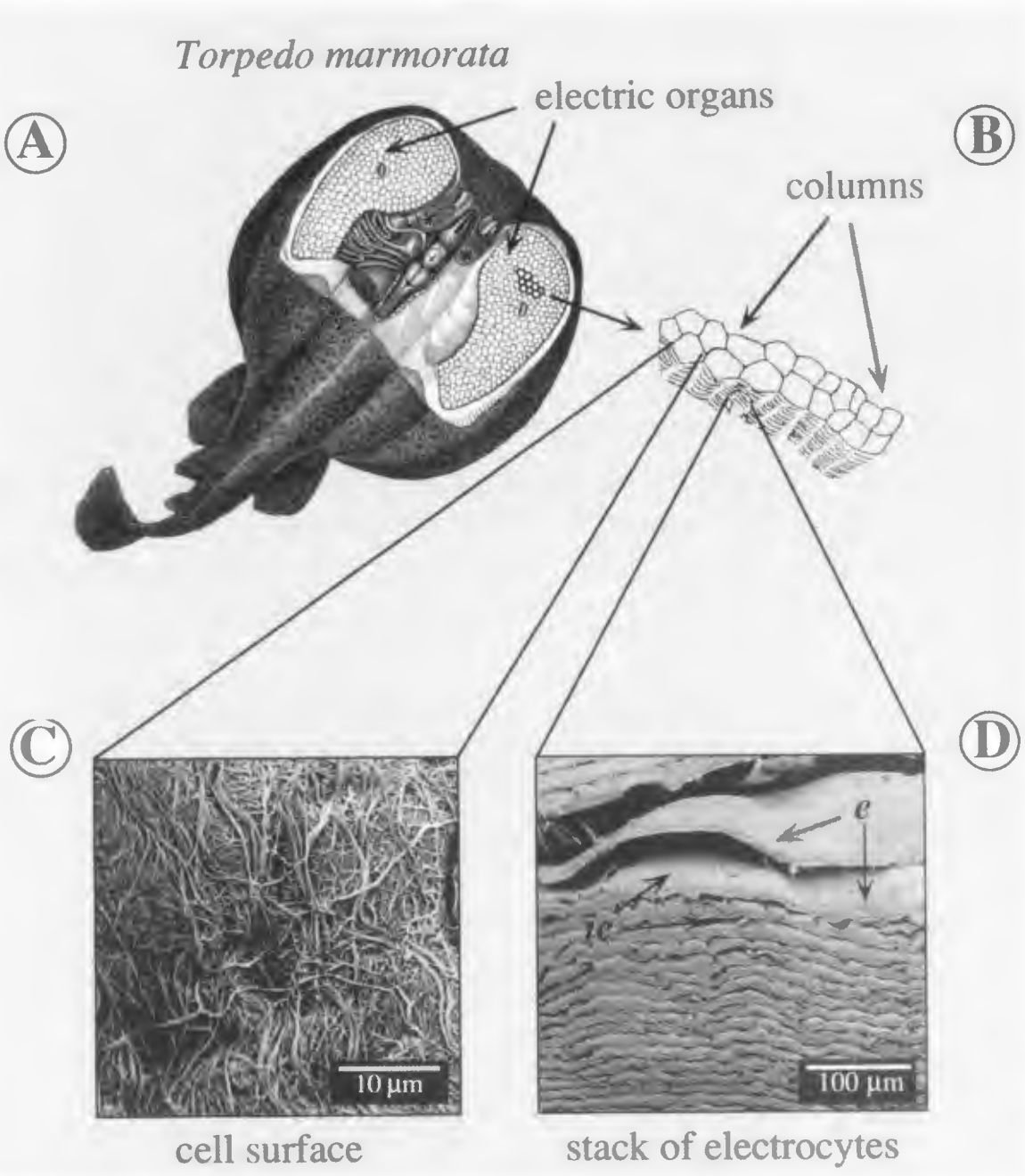

Figure 1. Electric organ from *Torpedo marmorata* imaged in the SEM. **(A)** Historical representation of a partially dissected *Torpedo marmorata* (Fritsch, 1890). Head-to-tail length: 25-40 cm. **(B)** Scheme of the arrangement of electrocytes within the electric organ. Individual electrocytes are stacked and are organized into columns. **(C)** Scanning electron micrograph of critical-point dried cell stack after longitudinal fracturing. **(D)** Overall morphology of a column after transversal cryosectioning in the SEM (e: electrocyte; ie: intercellular space).

---

appreciably reduced in fluid (Weisenhorn *et al.*, 1989). SFM imaging in liquid was carried out using a commercial fluid cell (DI) and without prior drying of the sample. All images were taken at a line scan rate of approximately 6 Hz. The standard planefit and flattening correction (3rd order fits) were applied to the data. The various images were combined and processed for presentation with the programs Photoshop (Adobe Systems, Mountain View, CA) and Canvas (Deneba Systems, Miami, FL) for the Apple Macintosh computer. Cross-

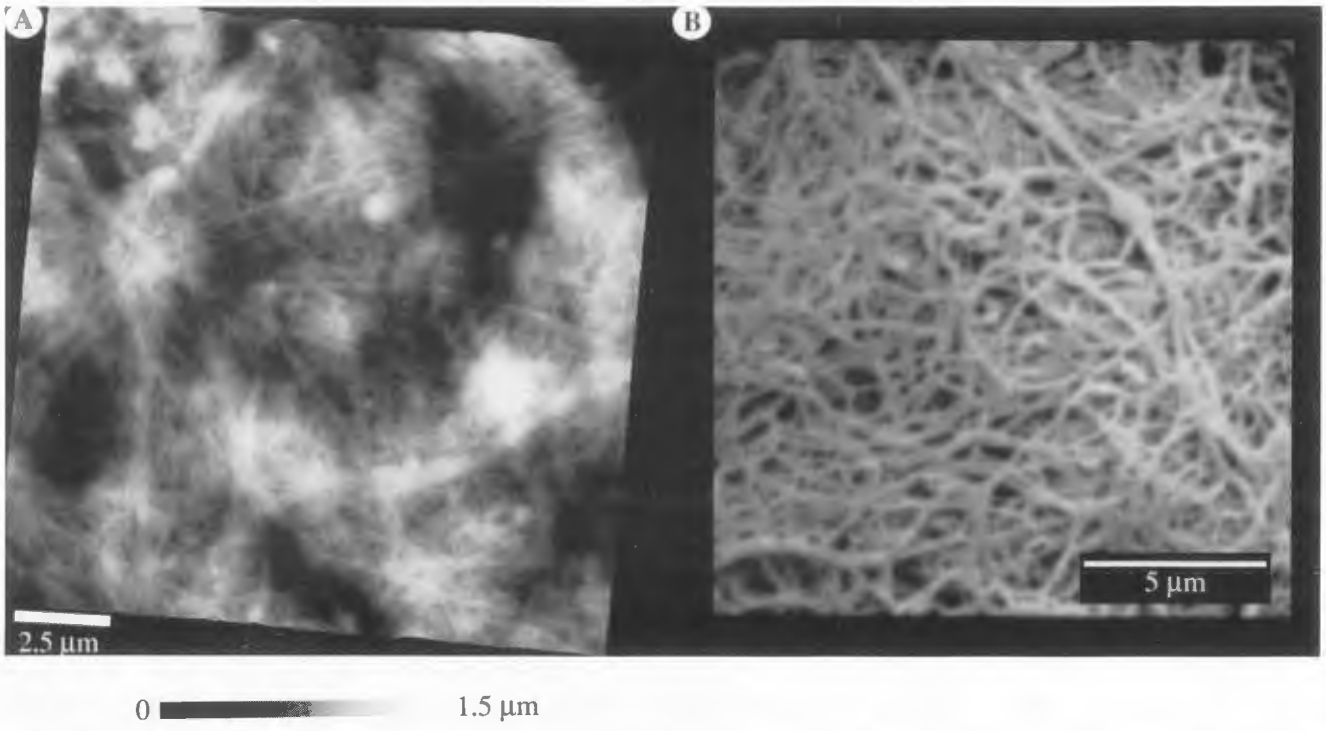

Figure 2. The cell surface of the sections is covered by a mesh of collagen fibers. **(A)** Scanning force micrograph of a selected surface area after longitudinal cleavage of the cell stack mounted between coverslips for fixation and critical point drying. A flat cleavage plane was exposed to the tip which revealed a dense network of collagen fibers. Perspective view (tilt 81°; rotation 5°). Tapping mode. Height information is coded in pseudo color according to the horizontal color bar. **(B)** Scanning electron micrograph of critical-point dried cell stack after longitudinal fracturing. Topview of cell surface of an electrocyte showing a dense fibrous feltwork.

sectional and Fourier transform analyses were performed with the NanoScope software. The reported lateral dimension of a surface feature is the full width at half maximum (FWHM) height determined by the sectioning software of the NanoScope, providing a practical and simple compromise between the point and face detection modalities of a tip (Fritzsche *et al.*, 1994a).

Immunofluorescence microscopy (IFM)

For immunofluorescence microscopy samples from transversal sections were washed with PBS and preincubated with 1% bovine serum albumin and 0.1% Triton-X100 in PBS for 15 minutes at room temperature in order to permeabilize the tissue section and to reduce nonspecific binding. The sample was stained for 1 hour with a monoclonal antibody (88B, kindly provided by Dr. S. Froehner) directed against the cytoplasmic domains of the γ and δ subunits of the AChR, and subsequently rinsed with 0.1% Triton-X100 in PBS. For secondary antibody labeling, tetramethylrhodamine-conjugated goat anti-mouse IgG (Jackson Immunoresearch, West Grove, PA) was applied. For AChR labeling, at the postsynaptic membrane of the electrocyte, fluorescein labeled α-bungarotoxin (Molecular Probes, Eugene, OR) was used in combination with the second antibody. The samples were rinsed with buffer and mounted with Mowiol 4-88 (Hoechst, Frankfurt, FRG). Fluorescence imaging was conducted using a confocal laser scanning microscope (CLSM, Zeiss model LSM 10, Zeiss Oberkochen, FRG; 40 × NA 1.3, Plan-Apo oil-immersion objective). Fluorescein and tetramethylrhodamine were excited at 488 nm and 514 nm, respectively, by an internal argon-ion laser. The emission filters were BP525 for fluorescein and LP610 for tetramethylrhodamine. Optical sections (8 bit) were acquired with frame averaging and transferred to a DEC Micro VAX II (Digital Equipment Corp., Palo Alto, CA), and subsequently to a Macintosh computer for contrast enhancement and image processing with the programs Photoshop, Canvas, and NIH-Image (National Institutes of Health, Bethesda, MD).

Results

Overall morphology of the electric organ and fluorescence labeling of the AChR receptor

In this study, we dissected the electric organ of

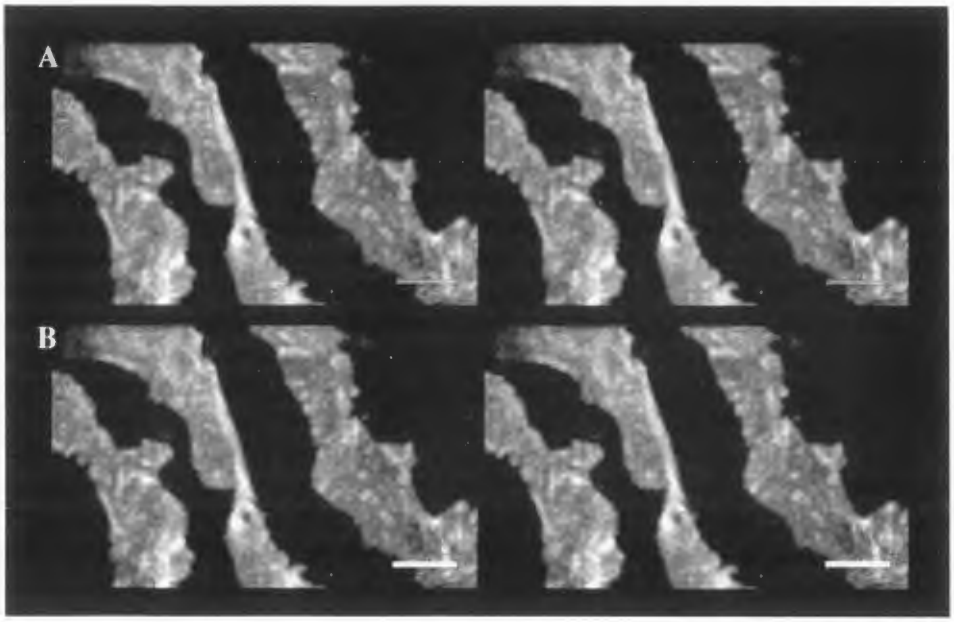

Figure 3. Fluorescence patterns in stereo representation of a tissue section after immunofluorescence labeling of the AChR. The thickness of the section was 8 μm. **(A)** Fluorescence patterns with the probe for the intracellular and **(B)** for the extracellular domains of the AChR, respectively. Bar = 10 μm. Mechanical distortions including twisting (central section) are apparent.

adult *Torpedo marmorata* (Figs. 1A, 1B and 1C) and examined the characteristic electrocyte morphology by SEM, SFM, and IFM. A typical scanning electron micrograph of a cross-section of an individual column of the electric organ is shown in Figure 1D. The column consists of a stack of individual electrocytes about 20 μm in width and separated by about 1-2 μm intercellular space. Electrocytes extend laterally over areas more than 1 cm wide, and the samples exhibit a pancake-like morphology. Cryoslicing (see below) was performed transversal to the cell stack (Fig. 1D). After longitudinal fracturing of a column, the cell surface was covered with fibers of different size (Fig. 1C), forming a dense network typical of collagen feltwork in connective tissue. For SFM, an alternative preparation procedure for frozen samples was devised to eliminate difficulties from folding of the tissue block during drying, a phenomenon which led to appreciable surface roughness (data not shown). The folding of the entire fixed and dried tissue block was a general problem for SFM imaging since: (i) the structural resolution normal to the surface was limited by the maximum **z** extension of the scanner, about 5 μm in our case; and (ii) fewer topographic features were accessible because of surface invagination and bulging, both of which increased the volume excluded from the tip and led to an apparent broadening of steeper structures. Significantly, improved sample stability was achieved by mounting the tissue block in a sandwich arrangement between polylysine coated coverslips prior to fixation and critical-point drying. Figure 2A shows a selected surface area after separation of the coverslips and surface cleavage by a sticky tape. The cleavage plane obtained parallel to the glass surface was amenable for imaging in the tens of μm range; that is, the surface corrugations were generally within the **z** limit of the scanner. The network of collagen fibers, visible during preparation, was resolvable by SFM (Fig. 2A) and thus similar to the SEM image in Figure 2B. In addition, some amorphous material was visible between the fibers, probably representing some form of cellular precipitate. We conclude that an appropriate and entirely unperturbed orientation of the tissue section could be easily and reproducibly achieved by the sandwich arrangement described above. The longitudinal fracturing of a column occurred preferentially between adjacent electrocytes. Our SEM and SFM data indicate that a thick collagenous sheath surrounds each electrocyte and also pervades the interelectrocyte space, i.e., effectively encasing the cell.

The functional surface of the electrocyte was also investigated. The subcellular distribution of AChR was determined by indirect IFM of cryostat sections of fixed tissue. Since the AChR is exclusively localized on the ventral surface such an essay should provide information about the orientation of the tissue. Simultaneous localization of different domains on the receptor molecule was achieved by double labeling experiments using fluorescein-conjugated α-bungarotoxin, a specific label for the extracellular domain of the α subunits (Fig. 3B), and the combination of a rhodamine-conjugated second antibody and the monoclonal antibody 88B directed against the intracellular domain of the AChR (Fig. 3A). From the fluorescence pattern in Figures 3A and 3B, it is obvious that the whole cell body was stained homogeneously. Thus, both the ligand binding site and intracellular epitope were accessible by the fluorescence probes, a consequence of the porous structure persisting after partial release of the cell contents and fixation, sectioning, and permeabilization. The intensity distribution suggests that

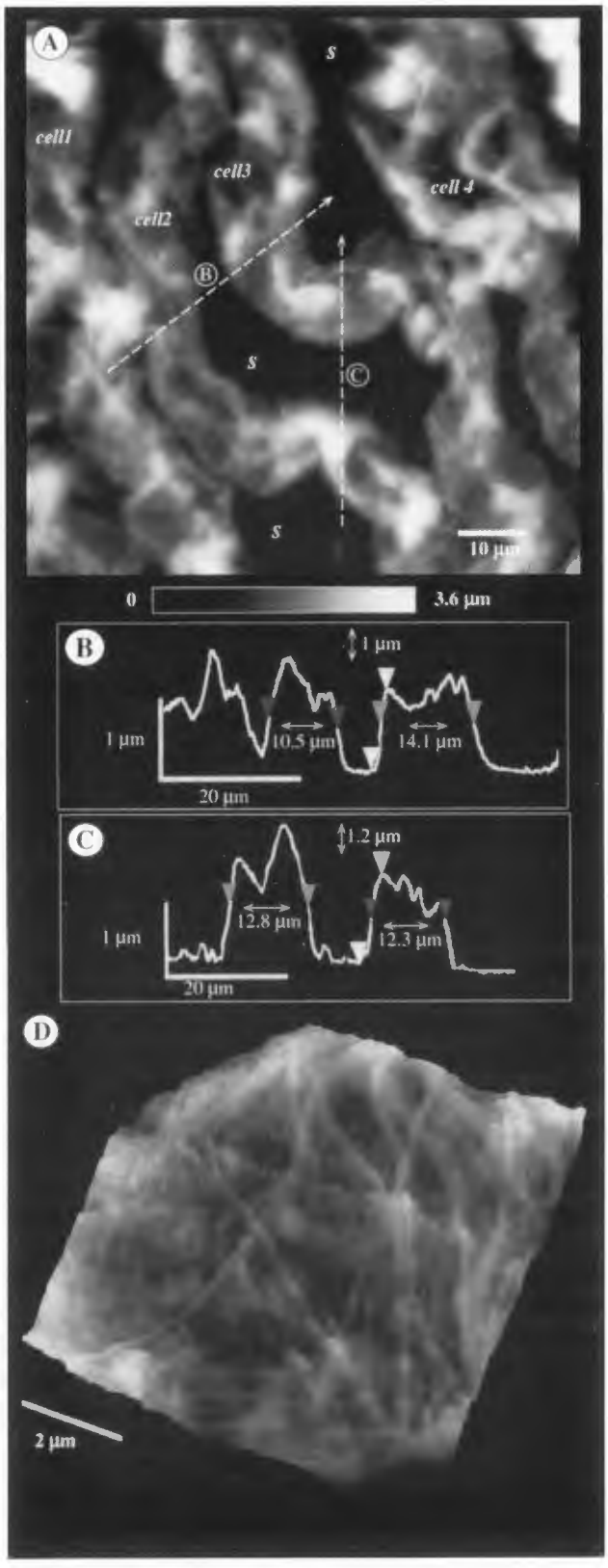

Figure 4. Overall morphology as revealed by SFM of a cryostat section from electric organ of *Torpedo marmorata*. The x,y dimensions are denoted by the horizontal bar and the height is color-coded according to the horizontal bar placed below the panels. Permanent contact mode. (**A**) Surface topography of the individual cells (**cell 1-4**) which exhibit a ribbon-like morphology. The glass surface is clearly visible in the intercellular space (s). (**B** and **C**) Cross-sections along the lines drawn in panel A. (**D**) Zoom and perspective view (tilt 69°; rotation 21°) of a region on an electrocyte.

the membrane surface was aligned parallel to the glass surface in contrast to the orientation of the cryosection plane (see **Discussion**).

The cell surface of the sections is covered by a mesh of collagen fibers

By SFM in air, we imaged transversal cross-sections after cryoslicing. Figure 4A shows an SFM image of a surface area with four individual cell bodies (cell 1-4) extending as a flat ribbon over the polylysine coated glass surface (s). The surface profile along lines B and C are presented in Figures 4B and 4C. From different images, we obtained a width of 9.6 ± 1.3 μm and a height of 1.3 ± 0.4 μm for the cell body of the electrocyte. Figure 4D shows the cell surface at higher resolution. A felt-work of collagen fibers covered the cell bodies. The bundles of collagen fibers appeared in a cross-striated pattern (Fig. 5A), indicating a role in the maintenance of the structural integrity of the columnar arrangement. Individual collagen fibers lying on the polylysine coated glass substrate in the vicinity from the cells were also perceived during imaging of the cryosections. The polylysine coated glass substrate appeared relatively flat with some oblate-shaped background protrusions of nanometer dimensions, presumably due to distortions from the coating (Vater *et al.*, 1995). Thus, the individual fibers were amenable to metrology. Their apparent width was about 150-170 nm and their height about 40-60 nm. This distinct deviation from the cylindrical fiber geometry was mainly due to drying artifacts and to SFM related distortions of the "real topography", including geometric tip-sample convolution and elastic (plastic) depression as discussed elsewhere (see e.g., Fritzsche *et al.*, 1994b; Vater *et al.*, 1995). A periodic substructure of the collagen fiber normal to the fiber long axis can be seen (Figs. 5A and 5B). Fourier transform analysis of the periodic pattern along the dashed line indicated in Figure 5C revealed a periodicity of 64 ± 2 nm (Fig. 5D). The topographic image of the collagen substructure (Fig. 5E) showed the corrugation amplitude along the collagen long axis to be 2.5 ± 1 nm.

Cryosections of the electric organ in liquid

We also performed SFM imaging of the tissue section in liquid without intermediate drying (Fig. 6). The

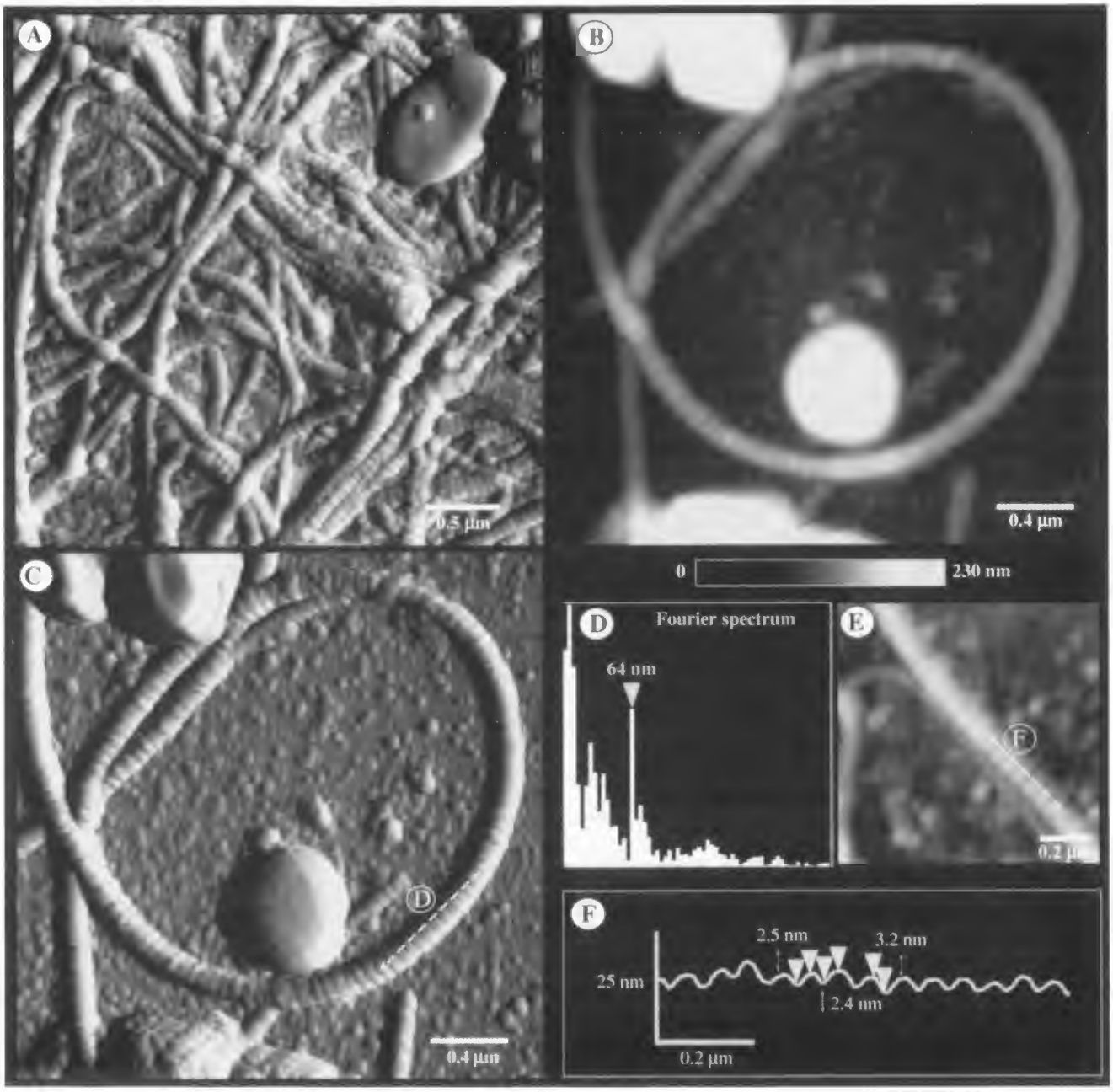

Figure 5. Collagen fibers from tissue sections imaged by SFM. **(A)** Area of a typical region with several cross contacts. Topview; error mode. **(B)** Structural details of an individual collagen fiber; isoforce mode. **(C)** Same fiber as in B imaged in error mode. This mode is more sensitive to changes in the surface relief. **(D)** The Fourier transform analysis along the dashed line indicated in panel C reveals a periodicity of 64 nm. **(E)** Zoom of a collagen fiber. **(F)** Cross-section along the line shown in panel E. The amplitude of the surface corrugations is 2.5 $\pm$ 1 nm.

intercellular spacing (Fig. 6A) was reduced, probably as a consequence of the hydration and volume increase of the cell body. From the cross-section (Fig. 6B), the cellular structures were about 16 μm in width (the thickness of the cut) and up to 3 μm in height. Upon comparison with the dried specimen, the sections exhibited greater structuring with prominent features and modulations. At higher magnification (Fig. 6C), the presence of fibers (presumably collagen since nerve fibers are typically > 1 μm in diameter) was apparent (arrows) but the spatial resolution was appreciably reduced compared to that of the dried sample. One reason for the loss of resolution

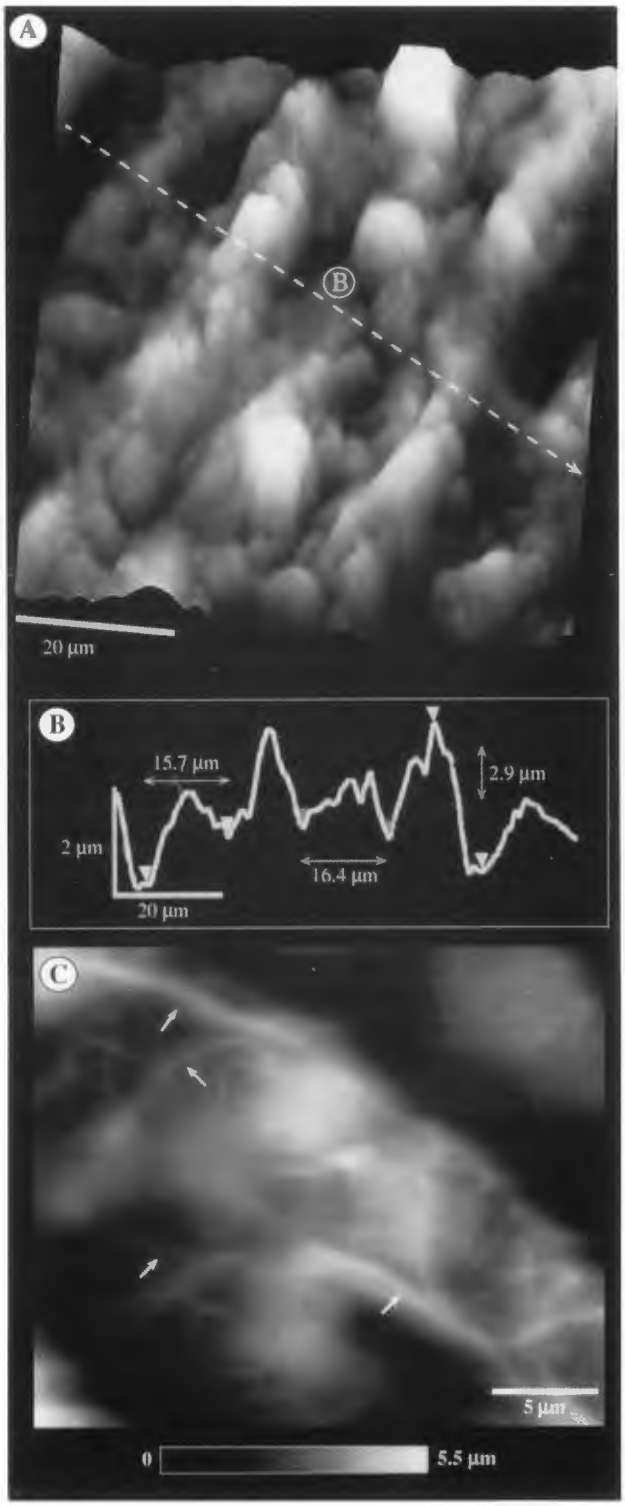

Figure 6. Cryosections of the electric organ imaged by SFM in liquid; isoforce mode. **(A)** Perspective view (tilt angle 81°; rotation 95°). **(B)** Cross-section along the line drawn in A. **(C)** Topview at higher magnification. The arrows point to a surface region where collagen fibers are evident.

could be that the hydrated complex biological material was soft and compliant under the tracking forces exerted by the tip (Fritzsche *et al.*, 1994b), a notion supported by the scan line distortions in Figure 6A. Such scanning artifacts are typically observed with heterogeneous patches varying in topological discontinuity and/or elasticity during the imaging of soft material. A second possibility is that the collagen matrix in the entire native structure encompasses the cell and is thus more confined to the interstitial spaces. The latter would tend to collapse upon drying of the sample.

Discussion

SFM reveals the "membrane surface view" of the thin section on the solid support

The unambiguous identification of orientation in tissue sections is of primary importance for the interpretation of fluorescence data. According to the SFM data in Figure 4, the thickness of the electrocyte cell body was about 1.5 μm with a lateral dimension of about 10 μm; furthermore, the cell body was covered with a felt-work of collagen. Since collagen lies between the stacked electrocytes of a column, it appeared that the tissue cryosections were tilted during deposition on the solid support and/or air drying. That is, the electrocyte membrane was exposed in a frontal orientation to the scanning tip and did not present as a cross-sectional plane through the cell bodies, contrary to the expectation from the initial orientation of the dissected tissue block. The thickness of a cell in a column after critical point drying was about 10 μm (Fig. 1D), i.e., 3-4 times larger than the height extracted from the surface profile of the hydrated tissue section in Figure 6C. We conclude that most of the cell content was released during sample preparation.

In the immunofluorescent pattern of Figure 3, the entire cell body appeared brightly stained after fluorescence labeling of the AChR. Such a pattern is contradictory to that expected for the AChR-rich ventral surface. That is, one would expect an anisotropic distribution of fluorescence intensity at the dorsal and ventral membranes. However, our experimental finding is in agreement with the tilted section hypothesis stated above, but not with the other proposals (Fiedler *et al.*, 1986; LaRochelle *et al.*, 1990) according to which the collapse of the cryostat sections produces so-called "*en face*" views of both the dorsal and ventral membranes after spreading and drying. Such a process involves a sliding of the dorsal and ventral membranes due to viscous drag during tilting of the section on the solid support, leading to uneven distribution of the AChR receptor at the dorsal and ventral membranes and thus an inhomogenous fluorescence intensity distribution at the cell

margins. From the entire data and considerations, it is obvious that the overall morphology of cryosections depends critically on the actual preparation conditions, e.g., constitution of the tissue, fixation, and orientation of the tissue block during slicing. Thus, care must be taken in interpreting fluorescence data of such specimens. A better approach for the determination of the polarity of the ventral and dorsal electrocyte membranes would be to embed the tissue in a solid matrix (Fox and Richardson, 1979; Zimmermann and Whittaker, 1974).

In situ observation of the collagen type I substructure by SFM

An important feature of our system was the observation of collagen *in situ*, inasmuch as this protein generally cannot be extracted from tissue without degradation because of existing chemical crosslink with the membrane (except for collagen from tail tendons of young rats). It is for this reason that SFM has been limited in previous experiments to the imaging of native isolated collagen fibers from rat tail and monomeric and reconstituted fibrillar collagen type I from bovine skin (Baselt *et al.*, 1993; Chernoff and Chernoff, 1992; Revenko *et al.*, 1994). In our system, the collagen remained associated with the cell membrane and details of the collagen fiber substructure could be obtained (Fig. 5).

The band pattern of the collagen substructure in the SFM images is similar to that perceived by transmission electron microscopy (Gelman *et al.*, 1979) and to images of isolated collagen type I fibers (Baselt *et al.*, 1993; Chernoff and Chernoff, 1992). The banding period was about 64 nm, in agreement with the structural parameters of the collagen type I fiber and the aggregation of tropocollagen into ordered arrays in the ridges and grooves (Hodge *et al.*, 1965). Our data indicate that collagen type I is the most abundant protein in the electric organ. The difference in height between the ridges and grooves normal to the collagen fiber long axis was about 2.5 nm, irrespective of the fiber diameter. This value is somewhat lower than the 4 nm reported by Revenko *et al.* (1994) and the measurements of Baselt *et al.* (1993), who recovered a peak-to-peak value between about 5 nm for small diameter fibrils and about 15 nm for large-diameter fibrils from rat tail tendon collagen. Since we used the same Si_3N_4 tips as in these cited studies, a similar three-dimensional resolution was to be expected. One possibility for the apparently smaller peak-to-peak height is that some material associated with the gap persisted during sample preparation according to our protocols.

Conclusion

We have shown that the structure of thin sections of the electric organ from *Torpedo marmorata* is amenable to study by SFM, yielding additional information on the morphological aspects of these preparations. The images obtained have nanometer spatial resolution and reveal molecular details conforming to the molecular substructure of collagen type I fibers in the tissue sections. The combination of electron, light, and probe microscopic techniques is emphasized, demonstrating their complementarity in the investigation of tissue structures. For future studies, one can hope to elucidate the native three-dimensional architecture by taking advantage of the potential for imaging under physiological conditions.

Acknowledgments

We are indebted to D. Kötting for technical assistance. This work was partly supported by the German Research Council (DFG; grants Jo 105/7 and Jo105/9), and by a grant from the Volkswagen Stiftung (grant I/70 887) to T.M.J. and F.J.B.

References

Barbee KA, Davies PF, Lal R (1994) Shear stress-induced reorganization of the surface-topography of living endothelial-cells imaged by atomic-force microscopy. Circ. Res. **74**: 163-171.

Baselt DR, Revel JP, Baldeschwieler JD (1993) Subfibrillar structure of type I collagen observed by atomic force microscopy. Biophys. J. **65**: 2644-2655.

Baumann A, Changeux JP, Benda P (1970) Purification of membrane fragments derived from non-excitable surface of the eel electroplax. FEBS Lett. **8**: 145-148.

Bennett MVL (1971) Electric Organs. In: Fish Physiology. Hoar WS, Randall DJ (eds.) Academic Press, Inc., New York. pp. 347-491.

Cartaud A, Jasmin BJ, Changeux JP, Cartaud J (1995) Direct involvement of a lamin-B-related (54 kDa) protein in the association of intermediate filaments with the postsynaptic membrane of the *Torpedo marmorata* electrocyte. J. Cell Sci. **108**: 153-160.

Chang L, Kious T, Yorgancioglu M, Keller D, Pfeiffer J (1993) Cytoskeleton of living, unstained cells imaged by scanning force microscopy. Biophys. J. **64**: 1282-1286.

Chernoff EAG, Chernoff DA (1992) Atomic force microscope images of collagen fibers. J. Vac. Sci. Technol. A **10**: 596-599.

Fiedler W, Borroni E, Ferretti P (1986) An immunohistochemical study of synaptogenesis in the electric organ of *Torpedo marmorata* by use of antisera to vesicular and presynaptic plasma membrane components. Cell Tissue Res. **246**: 439-446.

Fox GQ, Richardson GP (1979) The developmental

morphology of *Torpedo marmorata*: Electric organ-electrogenetic phase. J. Comp. Neurol. **185**: 293-316.

Fritsch G (1890) Uebersicht der Torpedineen (Overview of Torpedinidae). In: Die elektrischen Fische nach neuen Untersuchungen anatomisch-zoologisch dargestellt (The Electric Fish. Represented according to examinations of an anatomically-zoological manner). von Veit, Leipzig, Germany. pp. 10-53.

Fritz M, Radmacher M, Gaub HE (1994) Granula motion and membrane spreading during activation of human platelets imaged by atomic-force microscopy. Biophys. J. **66**: 1328-1334.

Fritzsche W, Schaper A, Jovin TM (1994a) Probing chromatin with the scanning force microscope. Chromosoma **103**: 231-236.

Fritzsche W, Schaper A, Jovin TM (1994b) Scanning force microscopy of chromatin fibers in air and in liquid. Scanning **17**: 148-155.

Gelman RA, Poppke DC, Piez KA (1979) Collagen fibril formation *in vitro*. The role of the nonhelical terminal regions. J. Biol. Chem. **254**: 11741-11745.

Hansma HG, Hoh JH (1994) Biomolecular imaging with the atomic-force microscope. Ann. Rev. Biophys. Biomol. Struct. **23**: 115-139.

Henderson E (1994) Imaging of living cells by atomic force microscopy. Progr. Surf. Sci. **46**: 39-60.

Hodge AJ, Petruska JA, Bailey AJ (1965) The subunit structure of the tropocollagen macromolecule and its relation to various ordered aggregation states. In: Structure and Function of Connective and Skeletal Tissue. Filton-Jackson S, Harkness RD, Partridge SM, Tristram GR (eds.). Butterworths, London. pp. 31-41.

Hoh JH, Hansma PK (1992) Atomic force microscopy for high-resolution imaging in cell biology. Trends Cell Biol. **2**: 208-213.

Hörber JKH, Häberle W, Ohnesorge F, Binnig G, Liebich HG, Czerny CP, Mahnel H, Mayr A (1992) Investigation of living cells in the nanometer regime with the scanning force microscope. Scanning Microsc. **6**: 919-930.

Kasas S, Gotzos V, Celio MR (1993) Observation of living cells using the atomic force microscope. Biophys. J. **64**: 539-544.

Kordelli E, Cartaud J, Nghiêm H-O, Pradel L-A, Dubreuil C, Paulin D, Changeux JP (1986) Evidence for a polarity in the distribution of proteins from the cytoskeleton in *Torpedo marmorata* electrocytes. J. Cell Biol. **102**: 748-761.

Kordelli E, Cartaud J, Nghiêm H-O, Changeux J-P (1987) *In situ* localization of soluble and filamentous actin in *Torpedo marmorata* electrocyte. Biol. Cell **59**: 61-68.

Kordelli E, Cartaud J, Nghiêm H-O, Devillers-Thiéry A, Changeux J-P (1989) Asynchronous assembly of the acetylcholine receptor and of the 43-kD ν1protein in the postsynaptic membrane of developing *Torpedo marmorata* electrocyte. J. Cell Biol. **108**: 127-139.

Lal R, Drake B, Blumberg D, Saner DR, Hansma PK, Feinstein SC (1995) Imaging real-time neurite outgrowth and cytoskeletal reorganization with an atomic-force microscope. Am. J. Physiol. **38**: C 275-285.

Lal R, John SA (1994) Biological applications of atomic-force microscopy. Am. J. Physiol. **266**: C1-21.

LaRochelle WJ, Witzemann V, Fiedler W, Froehner SC (1990) Developmental expression of the 43K and 58K postsynaptic membrane proteins and nicotinic acetylcholine receptors in *Torpedo* electrocytes. J. Neurosci. **10**: 3460-3467.

Luft JH (1958) The fine structure of the electric tissue. Exp. Cell Res. **5**: 168-182.

Miller C (1983) Integral membrane channels: Studies in model systems. Physiol. Rev. **63**: 1209-1242.

Parpura V, Haydon PG, Henderson E (1993a) Three-dimensional imaging of living neurons and glia with the atomic force microscope. J. Cell Sci. **104**: 427-432.

Parpura V, Haydon PG, Sakaguchi DS, Henderson E (1993b) Atomic force microscopy and manipulation of living glial cells. J. Vac. Sci. Technol. A **11**: 773-775.

Pietrasanta LI, Schaper A, Jovin TM (1994) Imaging subcellular structures of rat mammary carcinoma cells by scanning force microscopy. J. Cell Sci. **107**: 2427-2437.

Putman CAJ, van der Werf KO, de Grooth BG, van Hulst NF, Greve J, Hansma PK (1992) A new imaging mode in atomic force microscopy based on the error signal. In: Scanning Probe Microscopies. Manne S (ed.). SPIE, The International Society for Optical Engineering, Los Angeles, CA. pp. 198-204.

Putman CAJ, Degrooth BG, Hansma PK, Vanhulst NF, Greve J (1993a) Immunogold labels: Cell-surface markers in atomic force microscopy. Ultramicroscopy **48**: 177-182.

Putman CAJ, van Leeuwen AM, de Grooth BG, Radosevic K, van der Werf KO, van Hulst NF, Greve J (1993b) Atomic force microscopy combined with confocal laser scanning microscopy: A new look at cells. Bioimaging **1**: 63-70.

Radmacher M, Tillmann RW, Fritz M, Gaub HE (1992) From molecules to cells: Imaging soft samples with the atomic force microscope. Science **257**: 1900-1905.

Revenko I, Sommer F, Minh DT, Garrone R, Franc J-M (1994) Atomic force microscopy study of the collagen fibre structure. Biol. Cell **80**: 67-69.

Richardson GP, Fiedler W, Fox GQ (1987) Development of the electromotor system of *Torpedo marmorata*: Distribution of extracellular matrix and cytoskeletal

components during acetylcholine receptor focalization. Cell Tissue Res. **247**: 651-665.

Rosenbludt J (1975) Synaptic membrane structure in *Torpedo* electric organ. J. Neurocytol. **4**: 679-712.

Schoffeniels E (1959) Ion movements studied with single isolated electroplax. Ann. NY. Acad. Sci. **81**: 285-306.

Sealock RB, Kavookijan A (1980) Postsynaptic distribution of acetylcholine receptors in electroplax of the torpedine ray *Narcine brasiliensis*. Brain Res. **190**: 514-522.

Shao Z, Mou J, Czajkowsky DM, Yang J, Yuan J-Y (1996) Biological atomic force microscopy: What is achieved and what is needed. Adv. Phys. **45**: 1-86.

Sheridan MN (1966) The fine structure of the electric organ of *Torpedo marmorata*. J. Cell Biol. **24**: 129-141.

Shroff SG, Saner DR, Lal R (1995) Dynamic micromechanical properties of cultured rat atrial myocytes measured by atomic-force microscopy. Am. J. Physiol. **38**: C286-C292.

Vater W, Fritzsche W, Schaper A, Böhm KJ, Unger E, Jovin TM (1995) Scanning force microscopy of microtubules and polymorphic tubulin assemblies in air and in liquid. J. Cell Sci. **108**: 1063-1069.

Walker JH, Boustead CM, Witzemann V, Shaw G, Weber K, Osborn W (1985) Cytoskeletal proteins at the cholinergic synapse: Distribution of desmin, actin, fodrin, neurofilaments, and tubulin in Torpedo electric organ. Eur. J. Cell Biol. **38**: 123-133.

Weisenhorn AL, Hansma PK, Albrecht TR, Quate CF (1989) Forces in atomic force microscopy in air and water. Appl. Phys. Lett. **54**: 2651-2653.

White MM, Miller C (1979) A voltage-gated anion channel from the electric organ of *Torpedo californica*. J. Biol. Chem. **254**: 10161-10166.

Whittaker VP (1992) The electromotor system: Morphology and electrophysiology. In: The Cholinergic Neuron and its Target: the Electromotor Innervation of the Electric Ray *Torpedo* as a Model. Birkhaüser, Boston, MA. pp. 28-54.

Zimmermann H, Whittaker VP (1974) Effect of electrical stimulation on the yield and composition of synaptic vesicles from the cholinergic synapses of the electric organ of *Torpedo*: A combined biochemical, electrophysiological and morphological study. J. Neurochem. **22**: 435-450.

Discussion with Reviewers

M. Heim: Could you observe an increase in resolution when applying tapping mode? From many soft samples it is reported to improve the image stability and resolution by applying tapping mode in the liquid cell. Did you try tapping in liquids and what were your experiences?

Authors: Tapping mode is advantageous in the event that lateral (shear) forces exerted by the tracking tip on the surface topography result in image distortions. From our experience, a pronounced surface instability is not an intrinsic property of the biomaterial but rather derives from insufficient adhesion between the biomolecules and the solid support. Such behavior can be checked experimentally by switching between the permanent contact and tapping modes on the same surface area. We could not detect any difference in image contrast between the permanent contact and tapping modes, in agreement with other studies (cf. Vater *et al.*, 1995). However, this behavior depends on the actual sample or system under investigation and needs to be checked for every sample. We did not perform tapping in fluid with our samples.

Y. Lyubchenko: Can it be that intercellular filaments are made of other proteins similar to collagens or are they complexes of collagen type I and other proteins? Is there other direct evidence for this specific tissue that the filaments are exclusively the collagen filaments?

Authors: Collagen is the major component of the connective tissue between electrocytes. There are other components such as nerve fibers and blood vessels. We tried to image those structures but failed, probably due to their rare appearance and/or to their trapping within the collagen feltwork.

R. Lal: There are now AFMs available which allow for simultaneous multimodal imaging, including simultaneous light fluorescence and force microscopy. How difficult would it be to extend your work to such systems?

Authors: We believe that such combined studies would be useful, particularly for studying the distribution of the AChR. The receptor(s) can be localized by a fluorescence tag for fine positioning of the SFM tip. Such an approach is being implemented in our laboratory using a near-field scanning optical microscope (Kirsch *et al.*, 1996). However, one has still to get rid of the ubiquitous collagen. In an alternative approach, one could perform morphological studies on individual electrocytes obtained by enzymatic dissociation of the electric organ of some species of skate (Fox *et al.*, 1990).

R. Lal: Have you imaged at high resolution, in order to obtain the molecular structure of AChRs? If not, how difficult it would be to undertake such studies?

Authors: Due to the ubiquitous appearance of collagen, it is very difficult to access the cell without any additional surface treatment of the dissected tissue, e.g., by collagenase, or by other known methods of membrane purification. Such experiments would be a promising exten-

sion of our work since the ventral membrane is rich in the AChR. One could try to achieve the degradation of collagen in the fluid cell of the SFM. If one is only interested in resolving structural details of the AChR, a more appropriate system is offered by isolated membrane vesicles purified from the electric organ. Such vesicles are extremely rich in cholinergic receptor molecules (Heuser and Salpeter, 1979). The main problem in this approach is the sample preparation for the SFM since the highest resolution can only be achieved on flat surfaces. The possibility is to fuse the vesicles and collapse them on a flat support, such as mica, prior to imaging.

R. Lal: The images of collagen are great and every indication is that they are Type I. How difficult it would be to label them with Type I specific markers and show their regional distribution?

Authors: The immunolabeling of single collagen fibers would be possible (Fleischmajer *et al.*, 1990). However, we consider that the immunolabeling of this macromolecule in the complex three-dimensional tissue would be difficult to achieve.

Additional References

Fleischmajer R, MacDonald ED, Perlish JS, Burgeson RE, Fisher LW (1990) Dermal collagen fibrils are hybrids of type I and type III collagen molecules. J. Struct. Biol. **105**: 162-169.

Fox GQ, Kriebel ME, Pappas GD (1990) Morphological, physiological and biochemical observations on skate electric organ. Anat. Embryol. **181**: 305-315.

Heuser JE, Salpeter SR (1979) Organization of acetylcholine receptors in quick-frozen, deep-etched, and rotary-replicated *Torpedo* postsynaptic membrane. J. Cell Biol. **82**: 150-173.

Kirsch A, Meyer C, Jovin TM (1996) Integration of optical techniques in scanning probe microscopes: The scanning near-field optical microscope (SNOM). In: Proceedings of NATO Advanced Research Workshop: Analytical Use of Fluorescent Probes in Oncology. Kohen, E, Hirschberg, G (eds.). Plenum Press, New York. pp. 317-323.

Scanning Microscopy Vol. 10, No. 4, 1996 (Pages 975-982) 0891-7035/96$5.00+.25
Scanning Microscopy International, Chicago (AMF O'Hare), IL 60666 USA

FLUORESCENCE IMAGING AND SPECTROSCOPY OF BIOMATERIALS IN AIR AND LIQUID BY SCANNING NEAR-FIELD OPTICAL/ATOMIC FORCE MICROSCOPY

H. Muramatsu*, N. Chiba, K. Nakajima, T. Ataka, M. Fujihira[1], J. Hitomi and T. Ushiki[2]

Research Lab. for Advanced Tech., Seiko Instruments Inc., Takatsuka-shinden, Matsudo-shi, Chiba 271, Japan
[1]Dept. of Biomolecular Engineering, Tokyo Institute of Technology, Nagatsuta, Midori-ku, Yokohama 227, Japan
[2]Dept. of Anatomy and Histology, Niigata University School of Medicine, Asahimachi-dori 1, Niigata 951, Japan

(Received for publication April 1, 1996 and in revised form September 24, 1996)

Abstract

We have developed scanning near-field optical/atomic force microscopy (SNOM/AFM). The SNOM/AFM uses a bent optical fiber simultaneously as a dynamic force AFM cantilever and a SNOM probe. Resonant frequency of the optical fiber cantilever is 15-40 kHz. Optical resolution of the SNOM/AFM images shows less than 50 nm. The SNOM/AFM system contains photon counting system and polychrometer/intensified coupled charge devise (ICCD) system to observe fluorescence image and spectrograph of micro areas, respectively. Cultured cells were stained with fluorescein isothiocyanate (FITC)-labeled anti-keratin antibody or FITC-labeled phalloidin after treatment with Triton X-100. Fluorescence and topographic images were obtained in air and water. The fluorescence images showed clear images of keratin and actin filaments. The SNOM/AFM is perfect to observe biomaterials in liquid with a liquid chamber while the topographic Images showed subcellular structures which correspond to keratin and actin filaments.

Key Words: Actin filaments, atomic force microscopy, biomaterials, chromium, fluorescence imaging, keratin filaments, scanning near-field optical microscopy.

*Address for correspondence:
Hiroshi Muramatsu
Research Laboratory for Advanced Technology,
Seiko Instruments, Inc.,
Takatsuka-shinden, Matsudo-shi,
Chiba 271, Japan

Telephone number: 81-473-92-7880
FAX number: 81-473-92-7822
E-mail: muramatu@tk.sii.co.jp

Introduction

Scanning near-field optical/atomic force microscopy (SNOM/AFM) is an excellent tool to observe biological materials because it provides simultaneously topographic and optical images in high resolution. The resolution of topographic and optical images is much higher than that of the conventional far-field microscopy. Unlike electron microscopy, SNOM/AFM can observe samples in air and liquid. SNOM/AFM has also advantage to give various information such as fluorescence images and spectrographs in a micro area [7].

Various kinds of scanning near-field optical microscopy have developed in the variation of method to control tip-sample separation such as utilizing scanning transmission microscopy (STM) [5], lateral shear force [1], and contact-mode AFM [13, 15]. Aaron Lewis and coworkers originally developed SNOM/AFM using bent capillary tubes in which fluorescence material is settled on the tip of the tube to illuminate a sample surface [13]. After that, we developed the bent optical wave guide probe for the current type SNOM/AFM in which a method of the dynamic mode AFM was used to control the tip-sample separation [2, 9]. An optical fiber with a sharpened tip was bent for using the probe as a cantilever for AFM, and the vibration amplitude of the cantilever was held constant during scanning. The SNOM/AFM may be superior in biological observation to other SNOM systems because this system operates excellently in liquids [10]. It is safely applicable for observation of soft samples with great variations in height, such as cultured cells. The SNOM/AFM may also be superior in liquid to other cyclic contact AFM (e.g., tapping mode); the latter use flat type cantilevers [4, 6, 12], while the optical-fiber cantilever of SNOM/AFM is round, which helps to reduce viscositic resistance of liquid. In the case of the shear force mode, AFM may work in liquid but, to our knowledge, there are no published images of biological materials in liquid, such as cultured cells. In the tuning fork mode, where a tuning fork is used for the force detection of an optical fiber glued onto the fork [8], AFM needed improvement

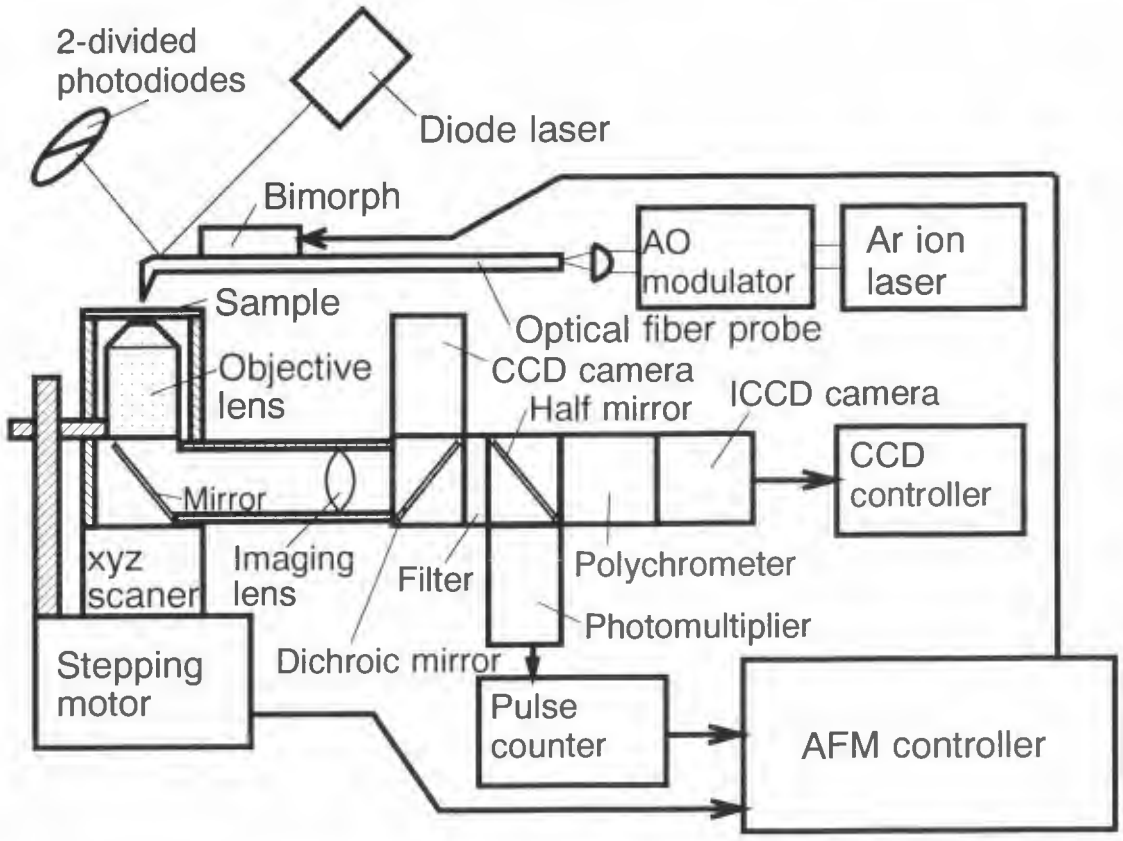

Figure 1. Schematic diagram of SNOM/AFM system.

for use in liquid because electrodes are patterned on the surface of the tuning fork, and electrical leakage would inhibit function in aqueous solution.

This paper reports the performance of SNOM/AFM in the observation of a standard specimen of chromium patterns and fluorescence beads and displays fluorescence SNOM/AFM images of cultured cells in the air and an aqueous solution.

Experimental Setup

The SNOM/AFM system is shown in Figure 1. The optical-fiber cantilever is mounted on a bimorph and vibrated vertically against the specimen stage at the resonant frequency (typically 15-40 kHz). The vibration voltage applied on the bimorph was between 0.1 and 5 $ACV_{p\text{-}p}$ for 0.11 nm/V bimorph. The vibration amplitude is monitored by detecting the deflection of the laser beam, which is reflected on the ground surface of the optical fiber cantilever. The probe tip-sample distance is controlled by decreasing the vibration amplitude to a appropriate level when the distance between the probe tip and the sample decrease. This operation was controlled by a commercialized AFM controller (model SPI 3700, Seiko Instruments, Chiba, Japan).

Laser beams of multi-line Ar ion laser (maximum 150 mW) were selected by polychromatic acoustic optical (AO) modulator and coupled to the optical fiber on the other side of optical fiber probe. Signal light from the sample is collected by objective lens (typically: 100 X oil immersion type) and separated by dichroic mirror to the coupled charge devise (CCD) camera and detectors. Photomultiplier and intensified-CCD camera with spectrometer are connected as the detectors.

Figure 2 shows a liquid chamber designed for the present experiment. Water and cell culture media were held between the glass plate and an upper window. Both the probe and the sample were immersed in solution.

The probe was prepared as previously described [2]. Briefly, an optical fiber, single mode for wavelength of 500 nm, was sharpened by chemical etching to make a tip, and then bent with irradiation of a CO_2 laser. The chemical etching is performed at room temperature for 45 minutes in 50% HF solution. CO_2 laser is at a maximum of 25 W and modulated to control power. Unfocused laser beam is used for bending. The probe was

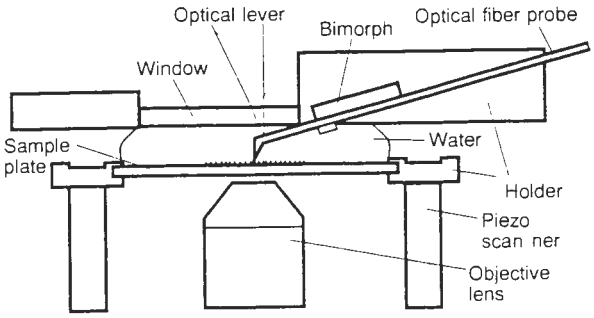

Figure 2. Schematic diagram of the liquid chamber in SNOM/AFM system.

coated with a 100-200 nm-thick metal layer (aluminum or gold), and an aperture was made by vapor deposition in rotating optical fiber tip (Fig. 3).

The spring constant was approximated by a spring constant equation for a rod:

$$k = \frac{3\pi d^4 E}{64 l^3} \qquad (1)$$

where k is the spring constant, d is the diameter of the rod, E is Young's modulus, and l is the length of the rod. A spring constant for 3 mm long probe was calculated at 97 N/m. Q factor is typically 200-600 in the air and 20-200 in water [11]. The oscillation amplitude employed was between 10-100 nm (0.1-1 ACV_{p-p} in the air, or 0.5-5 ACV_{p-p} in water for driving the bimorph). Under typical imaging conditions, average sample-probe separation was controlled by the amplitude of the vibration, which became 80-96% of the free vibration amplitude. The interaction force between the probe and the sample was as small as that of normal cyclic contact mode AFM.

The advantage of the instrument operating in liquid was proved by resonance curves of an optical fiber probe and a silicon cantilever in liquid. The resonance curve for the silicon cantilever showed many peaks and was not stable, but that for the optical fiber probe showed a clear single resonance peak in liquid, as seen in Figure 4.

Results and Discussion

Figures 5a and 5b show representative topographic and optical images of a standard sample observed with a 514.5 nm laser beam. The standard sample is a patterned chromium layer of 2 μm by 2 μm checker with 20 nm thickness on a quartz glass plate. In the topographic image, the higher part shows the chromium

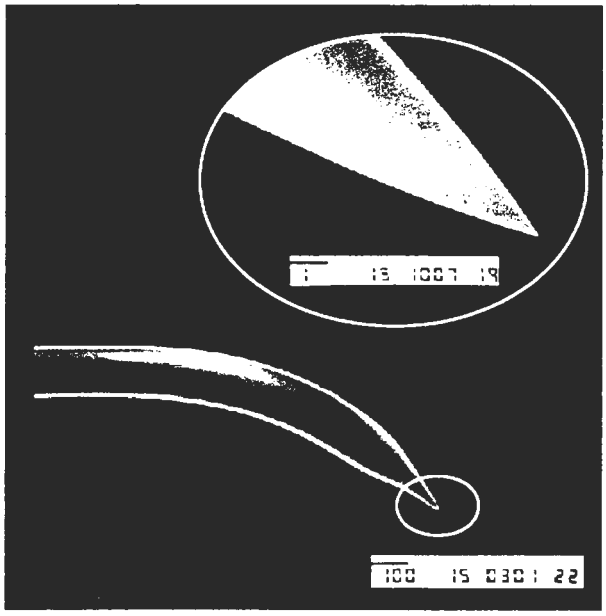

Figure 3. A representative scanning electron microscope image of the probe made from an optical fiber coated with aluminum.

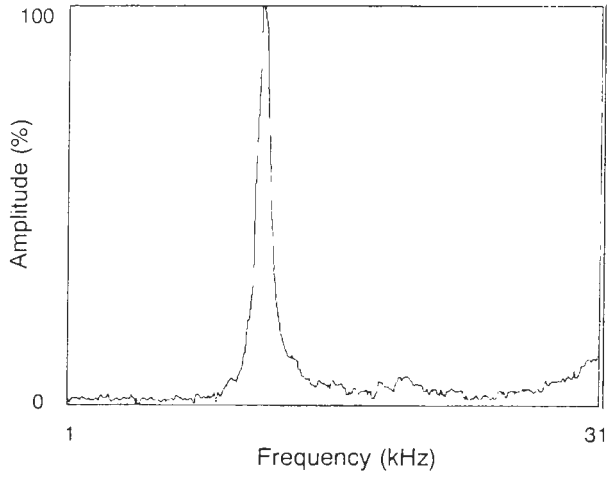

Figure 4. Typical resonance curve for the optical fiber cantilever in water. The resonant frequency is 12.2 kHz, and the Q factor is 23.

layer. The chromium layer produces dark parts in the optical image because the chromium layer blocks the transmitting a light from the optical fiber probe to the objective lens. In the SNOM/AFM operation, the laser beam was modulated with an AO modulator by the same frequency of probe vibration. The phase between probe vibration and irradiation cycle was tuned as the irradiation allows when the tip-sample separation is smallest in

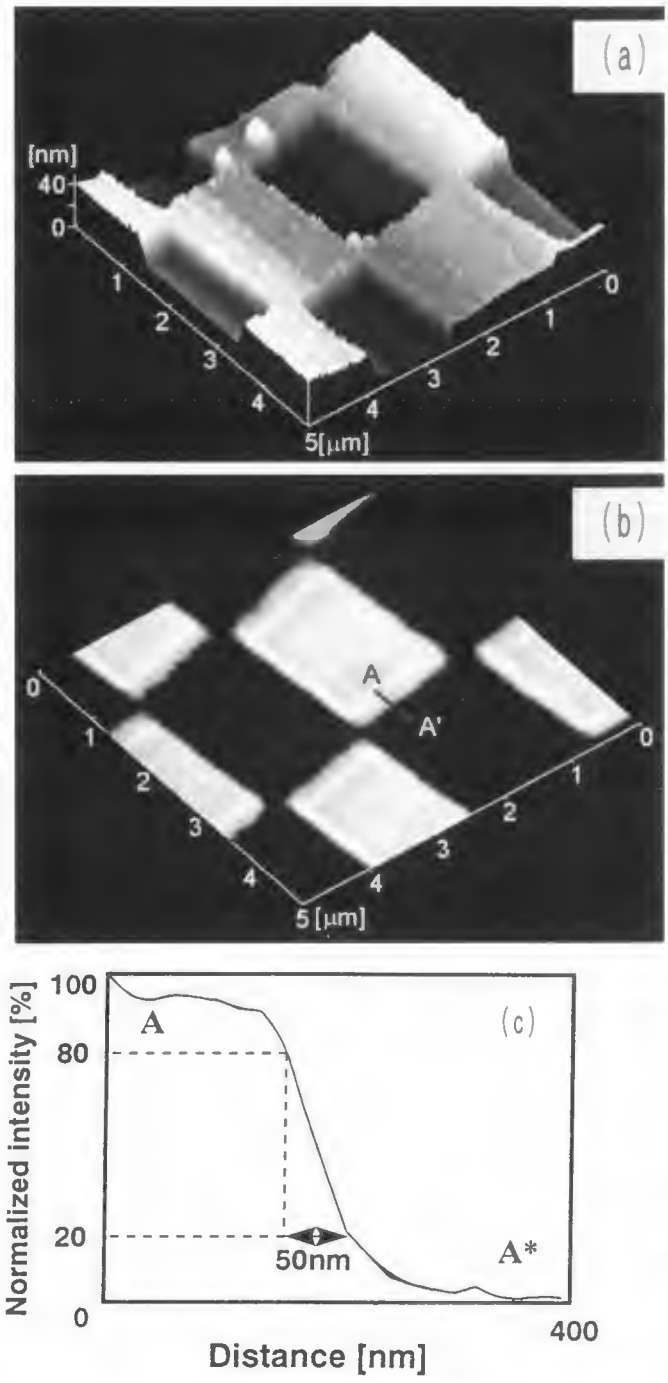

Figure 5. Topographic (a) and near-field optical (b) images of a standard chromium pattern on quartz glass plate. The optical profile (c) of A-A' in Figure 5b. A* of Figure 5c is equivalent to the A' of Figure 5b.

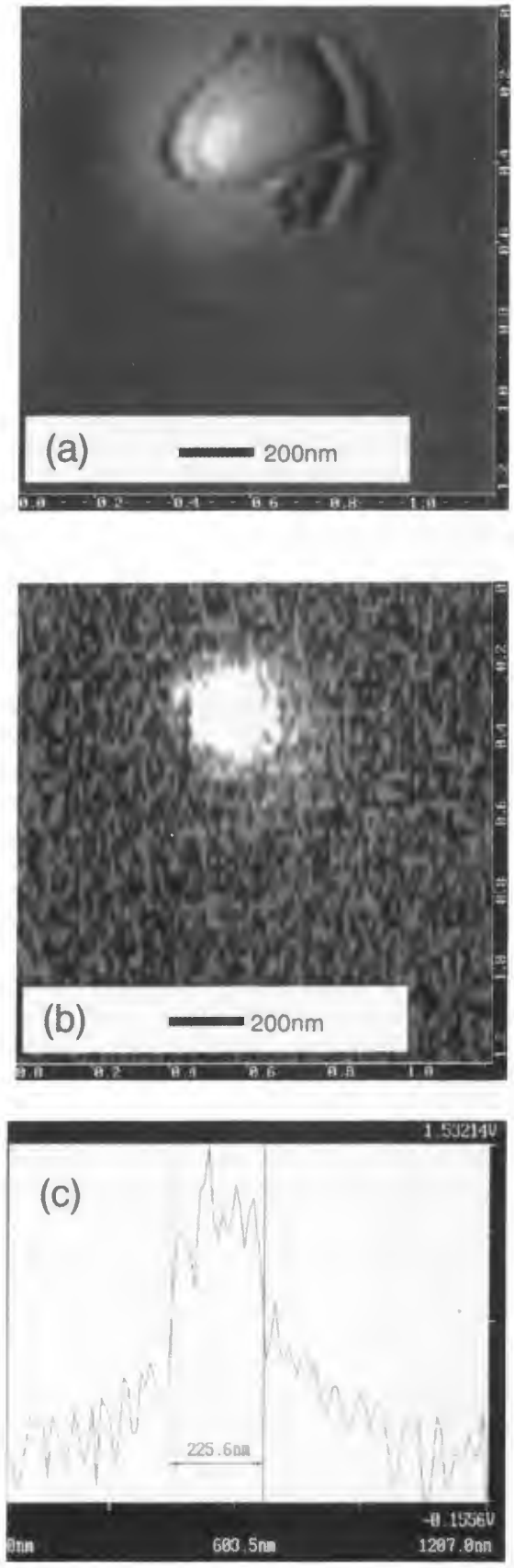

Figure 6 (at right). Topographic (a) and fluorescence (b) images of 100 nm fluorescence beads coated with PVA film on a cover glass. The fluorescence profile (c) of fluorescence of the beads in Figure 6b. Scan area is 1.2 μm by 1.2 μm.

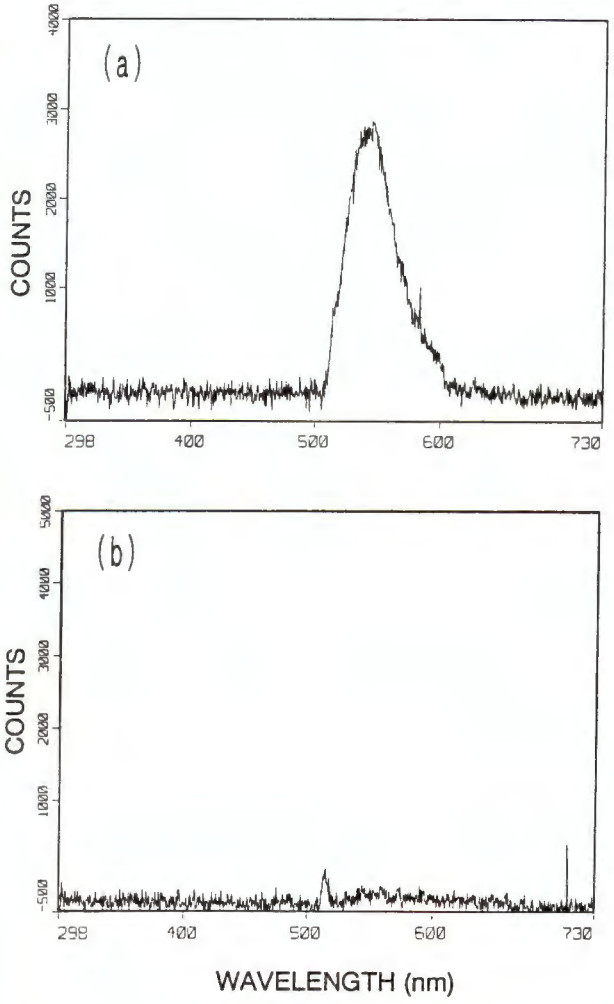

Figure 7. Spectrograph with 488 nm excitation when the probe tip was on the fluorescence beads (a) and 750 nm from the beads (b).

---

the vibration cycle. The separation between the tip and sample surface is a factor in the resolution of the optical image; for example, illuminating in wide separation decreases the optical resolution. When illumination is performed at the range of smallest separation during the vibration, the resolution will be kept in high level [3].

Figure 5c shows the optical profile which is marked as A-A' in Figure 5b. Generally, the resolution is defined as a distance of two particles or point-light-sources which can be imaged separately. In the case of point-light-sources, the distance of the two points should be slightly wider than the width of the half peak value (50%) of the gaussian profile which was detected by the probe. A width of 40% of the peak value enables a tip to image the two points separately. We applied this concept to the step of the metal layer. If the probe scans on a pin hole which is smaller than the aperture, the profile of optical image will be a reflected image of optical profile at intensity between 0% to 50%. The width of 20 to 80% in Figure 5c corresponds to the width of 40% of the left slope and 40% of the right slope of the peak in the reflected image. Actually, the width of the slope between the dark part and bright part shows 50 nm in 20-80% threshold.

When the probe tip is just on the edge of the chromium step, a half of the aperture is on the chromium layer while the other half of the aperture is 20 nm above the glass surface. This 20 nm distance is significant, particularly when considering the spreading of light at a coupling region of near field wave. Therefore, the aperture of the probe must be smaller than the width of slope, i.e., the aperture is smaller than 50 nm in this result.

In the fluorescence measurement, we used the photon counting type photomultiplier instead of the analog type photomultiplier in the transmission mode. Topographic and fluorescence images of 100 nm fluorescence beads are shown in Figures 6a and 6b, where beads were spread on cover glass with poly-vinyl-alcohol (PVA) film by spin coating the beads and PVA solution mixture to control the density of the beads on the glass plate. The PVA film was prepared thinner than the height of beads to enable the tip imaging topography and optical image of beads. The topographic image shows a round shape of beads and wrinkles of PVA film around the beads. The fluorescence image was observed with a 488 nm laser beam for excitation and showed the clear round shape of the fluorescence beads. The profile of fluorescence intensity of Figure 6b shows that the width of the fluorescence peak for the beads is about 200 nm (Fig. 6c). In this case, the diameter of the beads is 100 nm. In the fluorescent beads experiment, we used a probe which showed 100 nm resolution of our step sample, therefore, this result is reasonable. Scattering light produced at probe tip and sample surface may cause the slope of the fluorescence profile of the beads extending about 500 nm to the right and to the left of the peak. The slope profile may depend on the structural factor of the probe and sample surface.

Figure 7a is a fluorescence spectrograph, taken when the probe tip was on the fluorescence beads. In this experiment, the spectrum window is limited to a 515 to 600 nm range, because the system has a dichroic mirror of 500 nm and long wave pass filter of 515 nm to cut the excitation light, and short wave pass filter of 600 nm to cut the laser beam of optical lever (670 nm). The long wave pass filter will be removed when a self-sensitive probe, such as the tuning fork probe, is used. When the probe tip was located at 750 nm of lateral movement from the center of the beads, the spectrograph showed only a small peak of 514.5 nm (Fig. 7b). This

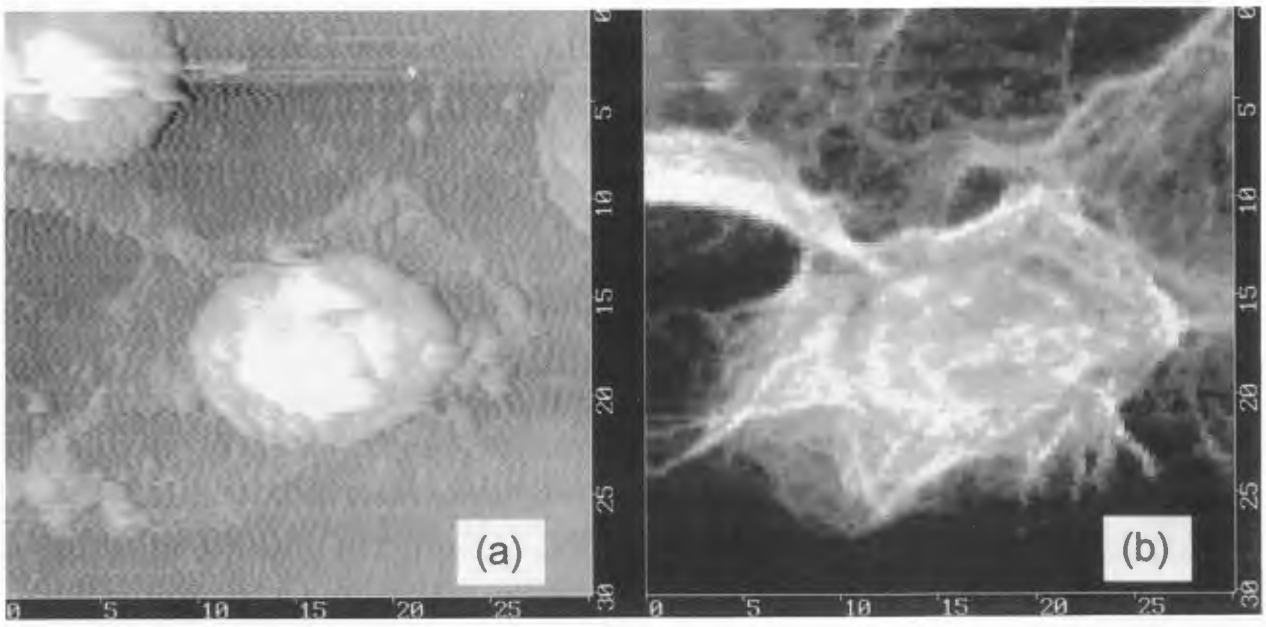

Figure 8. Topographic (a) and fluorescence (b) images of cultured cells of human esophageal squamous cell carcinoma (KESC2, C7) in the air in which cell were stained with FITC-labeled phalloidin after treatment with Triton X-100. Scan area is 30 μm by 30 μm.

peak was caused by leaking of the 514.5 nm beam from the polychromatic AO modulator, and easily cut by adding a band pass filter of 488 nm next to the AO modulator. This result shows that SNOM/AFM can obtain spectrograph in a submicron area. This function may be useful in analytical applications in biology and other fields.

Fluorescence and topographic images of cultured cells immunostained with fluorescein isothiocyanate (FITC)-labeled anti-keratin antibody or FITC-labeled phalloidin were obtained in air and water. Figures 8a and 8b show topographic and fluorescence images of cultured cells of human esophageal squamous cell carcinoma (KESC2, C7 subclone) in the air. The cells cultured on collagen-coated cover glass were treated with 1% Triton X-100, stained with FITC-labeled phalloidin and air dried. The topographic image is deteriorated in quality compared with that by normal dynamic mode AFM [14], but it clearly shows the shape of the cell nuclei. On the other hand, the fluorescence image shows actin filaments patterns with high resolution.

Figure 9 shows topographic and fluorescence images of the cultured cells (KESC2, C7) which were immunostained with FITC-labeled anti-keratin antibody after treatment of 1% Triton X-100, and observed by SNOM/AFM in aqueous solution. The fluorescence image shows the precise arrangement of keratin filaments. The topography apparently shows structures corresponding to keratin filaments as well as round cell nuclei.

The optical images in Figures 8 and 9 recorded 128 lines and 85 pixels per line for a scan of approximately 15 minutes. The images were not displayed to demonstrate optical resolution but to show a possibility of fluorescence imaging in liquid. The appearance resolution from images strongly depends on the sample itself.

The difference of fluorescence images in Figures 8 and 9 is caused because actin filament is a straight structure and keratin filament is a curled structure. Topographic images in Figure 9 show more natural structure than the image in Figure 8, which is a dried up structure. It is better to image the living or nearly living state to obtain the real structure. Therefore, observation of cultured cells is desirable to perform in liquid.

The importance of SNOM/AFM for simultaneous imaging of topography and fluorescence image should be noticed. It enables us to compare topography and fluorescence image. The interest of the cellular specimens is in the display of filament structure, as well as in the distribution of actin and keratin molecules in the cells.

Thus, SNOM/AFM introduces a new method for the study of cellular structures at high resolution unobtainable by conventional optical microscopy. This technique may reveal cell characteristics which are undetected by optical or electron microscopy. In addition, this study suggests that the SNOM/AFM system is widely applicable to specimens in water and other fluid media.

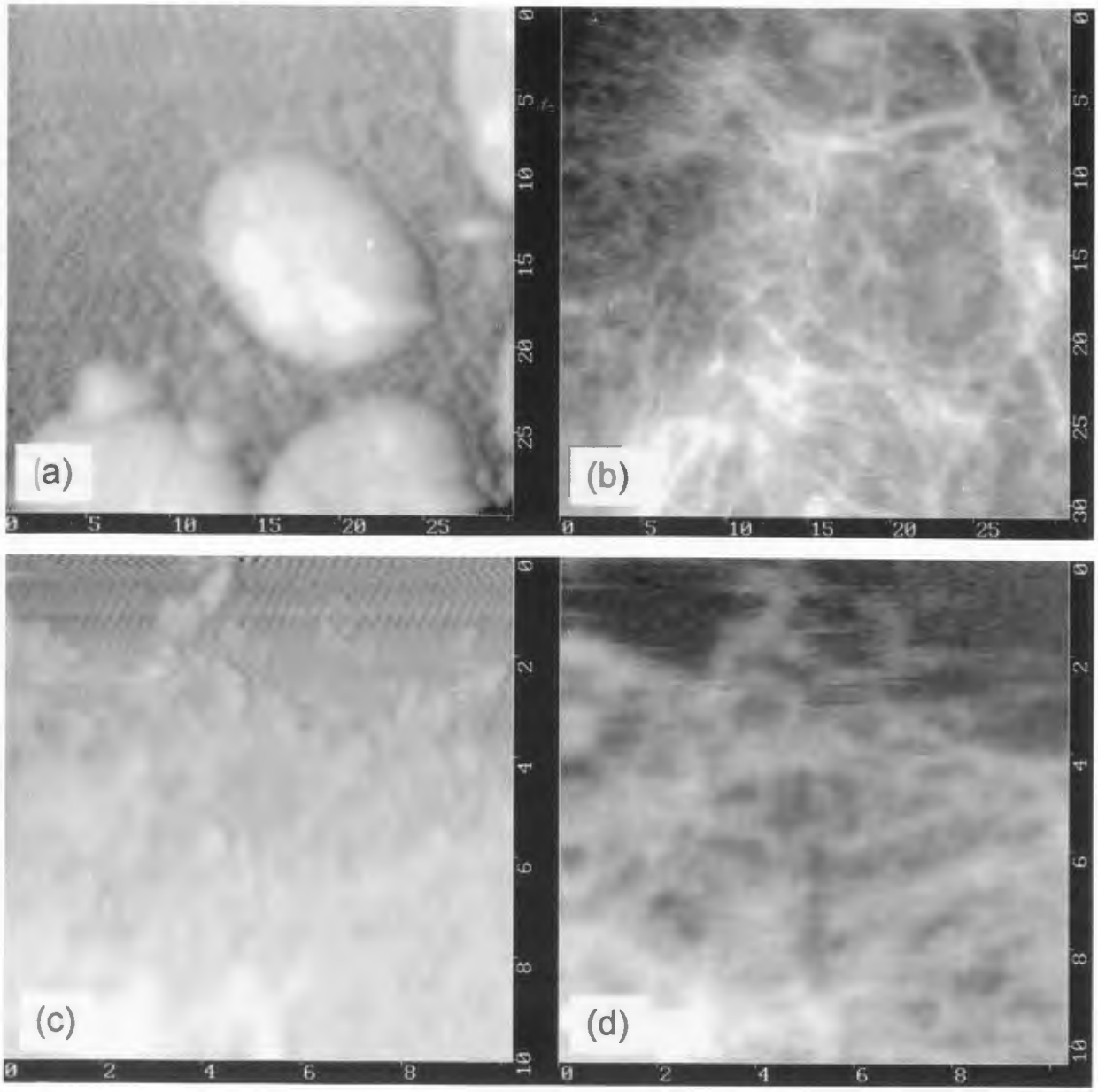

Figure 9. Topographic (**a** and **c**) and fluorescence (**b** and **d**) images of cultured cells of human esophageal squamous cell carcinoma (KESC2, C7) in an aqueous solution, in which cells were stained with FITC-labeled anti-keratin antibody after treatment with Triton X-100. Scan areas are 30 μm by 30 μm (**a** and **b**) and 10 μm by 10 μm (**c** and **d**).

References

[1] Betzig E, Trautman JK (1992) Near-field optics: Microscopy, spectroscopy, and surface modification beyond the diffraction limit. Science **257**: 189-195.

[2] Chiba N, Muramatsu H, Ataka T, Fujihira M, (1995) Observation of topography and optical image of optical fiber end by atomic force mode scanning near-field optical microscope. Jpn J Appl Phys **34**: 321-324.

[3] Chiba N, Muramatsu H, Nakajima K, Homma K, Ataka T, Fujihira M (1995) Resolution of an optical image of a scanning near-field optical/atomic force microscope as a function of sample-probe distance during synchronized irradiation. Thin Solid Films **273**: 331-334.

[4] Dreier M, Anselmetti D, Richmond T, Dammer

U, Güntherodt HJ (1994) Dynamic force microscopy in liquids. J Appl Phys **76**: 5095-5097.

[5] Dürig UT, Pohl DW, Rohner F (1986) Near-field optical-scanning microscopy. J Appl Phys **59**: 3318-3327.

[6] Hansma PK, Cleveland JP, Radmacher M, Walters DA, Hillner PE, Bezanilla M, Fritz M, Vie D, Hansma HG (1994) Tapping mode atomic force microscopy in liquids. Appl Phys Lett **64**: 1738-1740.

[7] Heinzelman H, Pohl DW (1994) Scanning near-field optical microscopy. Appl Phys A **59**: 89-101.

[8] Karrai K, Grober RD (1995) Piezoelectric tip-sample distance control for near field optical microscopes. Appl Phys Lett **66**: 1842-1844.

[9] Muramatsu H, Chiba N, Ataka T, Monobe H, Fujihira M (1995) Scanning near-field optic/atomic force microscopy. Proceedings of second conference on near-field optics, Raleigh, NC, 20-22 October 1993. Ultramicroscopy **57**: 141-146.

[10] Muramatsu H, Chiba N, Homma K, Nakajima K, Ataka T, Ohta S, Kusumi A, Fujihira M (1995) Near-field optical microscopy in liquids. Appl Phys Lett **66**: 3245-3247.

[11] Muramatsu H, Chiba N, Umemoto T, Homma K, Nakajima K, Ataka T, Ohta S, Kusumi A, Fujihira M (1995) Development of near-field optic/atomic force microscopy for biological materials in aqueous solutions. Ultramicroscopy **61**: 265-269.

[12] Putman CAJ, Van der Werf KO, De Grooth B G, Van Hulst NF, Greve J (1994) Tapping mode atomic force microscopy in liquids. Appl Phys Lett **64**: 2454-2456.

[13] Shalom S, Lieberman K, Lewis A (1992) A micropipette force probe suitable for near-field scanning optical microscopy. Rev Sci Instr **63**: 4061-4065.

[14] Ushiki Y, Shigeno M, Abe K (1994) Atomic force microscopy of embedment-free sections of cells and tissues. Arch Histol Cytol **57**: 427-432.

[15] van Hulst NF, Moers MHP, Noordman OFJ, Tack RG, Segerink FB, Bölger B (1993) Near-field optical microscope using a silicon-nitride probe. Appl Phys Lett **62**: 461-463.

Editor's Note: All of the reviewer's concerns were appropriately addressed by text changes, hence there is no **Discussion with Reviewers**.